Journal of Macromolecular Science, Part A
Publication details, including instructions for authors and subscription information:
http://www.informaworld.com/smpp/title~content=t713597274

Magnetic Polymer Composite Particles Via *In situ* Inverse Miniemulsion Polymerization Process

Hazem El-Sherif[a]; Mansour El-Masry[a]; Hassan Salah Emira[a]
[a] Polymers and Pigments Department, National Research Center, Dokki, Cairo, Egypt

Online publication date: 21 September 2010

To cite this Article El-Sherif, Hazem , El-Masry, Mansour and Emira, Hassan Salah(2010) 'Magnetic Polymer Composite Particles Via *In situ* Inverse Miniemulsion Polymerization Process', Journal of Macromolecular Science, Part A, 47: 11, 1096 — 1103
To link to this Article: DOI: 10.1080/10601325.2010.511523
URL: http://dx.doi.org/10.1080/10601325.2010.511523

Journal of Macromolecular Science, Part A: Pure and Applied Chemistry (2010) **47**, 1096–1103

ISSN: 1060-1325 print / 1520-5738 online
DOI: 10.1080/10601325.2010.511523

Magnetic Polymer Composite Particles Via *In situ* Inverse Miniemulsion Polymerization Process

HAZEM EL-SHERIF*, MANSOUR EL-MASRY and HASSAN SALAH EMIRA

Polymers and Pigments Department, National Research Center, Dokki, Cairo, Egypt

Received May 2010, Accepted June 2010

We aimed at preparing magnetic iron oxide particles by the oxidation-precipitation method in order to encapsulate these particles in polymer matrices composed of poly(acrylamide-styrene sulfonic acid sodium salt). Nanocomposites were synthesized by the incorporation of surface treated magnetic nanoparticles in the synthesized polymers via *in situ* inverse mini-emulsion polymerization process. The study parameter was the ionic monomer content in the synthesized polymers. The structure and the morphology of the magnetic nanogels were characterized by Fourier transform infrared spectroscopy (FTIR), X-ray diffraction (XRD), dynamic light scattering (DLS), thermal gravimetric analysis (TGA) and scanning electron microscopy (SEM). FTIR and XRD showed that pure magnetite was formed and successfully encapsulated in the composite nanoparticles. The polymer encapsulation could reduce the susceptibility to leaching and could protect the magnetite particle surfaces from oxidation. The ionic monomer content had a great effect on the magnetization behavior. Magnetite prepared by the oxidation precipitation method, of 50 nm mean particle size, was embedded successfully into the polymer nanogels with a reasonable magnetic response, as proved by vibrating sample magnetometer measurement. Magnetic nanocomposites were proven to be super-ferromagnetic materials.

Keywords: Inverse mini-emulsion polymerization, magnetite, magnetic polymer composite, encapsulation, polymer nanogels

1 Introduction

The synthesis of hybrid materials, by encapsulating inorganic material in a polymer matrix, opens new possibilities in the fabrication of solid particles for materials science, and is also of great interest in pharmaceutical and biotechnological industries, especially for producing drug release products. However, recent studies have underlined the major difficulty to encapsulate inorganic particles homogeneously, especially in the case of magnetic particles in polymer microgels (1). Different inorganic or polymeric materials have been proposed as carriers of magnetic materials. A considerable advantage of the polymeric carriers is the presence of a variety of functional groups, which is able to modulate the carrier properties for the desired applications (2,3). Ferromagnetic materials embedded in suitable matrices might be used in environmental applications (e.g. wastewater treatment) (4), in biotechnology (e.g. cell separation, immunoassay and nucleic acids concentration) or in medicine (e.g. separation of micro-organisms, detoxification of biological fluid and magnetic guidance of particle systems for specific drug delivery process) (5) or in other applications such as magnetic storage media, printing inks, magnetic resonance imaging, biosensors and catalysis (4–6).

The preparation of magnetite/polymer particles could be generally classified into three categories. One method was to assemble magnetic particles and polymer microspheres after they were synthesized separately, which afforded composite particles with magnetic properties via physical or physicochemical interaction between these two components. The second technique was the *in situ* precipitation of iron-oxides in the presence of polymer microspheres. The third way was to *in situ* polymerize monomers in the presence of magnetic particles (6). Heterogeneous polymerization was the most extensive and effective method to encapsulate magnetic particles to prepare magnetic polymeric composite particles (7), including conventional emulsion polymerization (8), miniemulsion polymerization (9), inverse emulsion/microemulsion polymerization (5,10), emulsifier-free miniemulsion polymerization (11), seeded emulsion polymerization(7) and suspension polymerization (4,12). Generally, encapsulation of magnetite in polymer particles cannot only inhibit iron leaking and oxidization of magnetite, but also give high colloidal stability, high magnetite content, and some desirable functional groups on the particle surface (9).

Magnetic particles are usually composed of the magnetic cores to ensure a strong magnetic response and a polymeric

*Address correspondence to: Hazem El-Sherif, Polymers and Pigments Department, National Research Center, El-Bohouth St., Dokki, Cairo, Egypt. Tel: 0020102227643; E-mail: elsherifhazem@hotmail.com

shell to provide favorable functional groups and features for various applications (3). The shell prevents the Fe_3O_4 core from oxidation and aggregation. With good hydrophilicity and biocompatibility, magnetic nanogels with a hydrogel shell can be desirable for biomedical applications, like drug delivery systems (13). The hydrophilic magnetic latexes have been first reported by Kawaguchi et al. by using acrylamide as the main monomer (5).

Magnetite nanoparticles were first produced in the 1960's by grinding iron oxides with surfactants and long chain hydrocarbons. This was followed by the development of precipitation techniques utilizing the reaction of soluble iron salts with a base (14). This method has been employed to create magnetite particles functionalized with a array of materials including water soluble polymers such as chitosan (3) and poly(vinyl alcohol) (15), nonpolar materials such as polystyrene (7,16) and poly(methyl methacrylate) (17). Other techniques have also proven successful for synthesizing magnetite nanoparticles. These include the use of microelmulsions (i.e., reverse micellar solutions) (18), hydrolyzation (19), polyol reductions (20), and elevated temperature decompositions of organic precursors (21). Among these methods, the chemical co-precipitation may be the most promising one because of its simplicity and productivity (22).

In this manuscript, oxidation precipitation method was performed to prepare magnetite. In order to study the magnetic response of polymer composites, the as-prepared magnetite was encapsulated in acrylamide-styrene sulfonic acid sodium salt (Am-SSASS) microgels via the *in situ* inverse miniemulsion polymerization technique. Various analytic techniques, traditionally applied in studies on polymer composites, such as FT-IR, X-ray, TEM, SEM and TGA, were performed to study these composites.

2 Experimental

2.1 Materials

Am was purchased from S.D. Fine Chemical, Ltd., Boisar, India. SSASS, ethylene glycol dimethacrylate (EGDMA), ammonium persulphate (APS) and Tween 60 were purchased from Aldrich-Chemical Co., Gillingham-Dorest, England. Span 60 and ferrous sulfate heptahydrate ($FeSO_4{\cdot}7H_2O$) were purchased from Fluka, Neu-Ulm, Germany. Oleic acid was from Merck. All the chemicals were of analytical grade and were used without further purification.

2.2 Techniques

2.2.1. *Preparation of Magnetic Iron Oxide by the Oxidation Precipitation Method*

$0.015\,mol.L^{-1}$ $FeSO_4{\cdot}7H_2O$ was divided into two parts. The first part was bubbled with O_2 at RT with vigorous stirring while the second one was heated at 80°C. Then, the two parts were mixed together and diluted NH_4OH solution (4%) was then added quickly to the solution at 80°C under vigorous stirring for 10 min. During the reaction process, the pH was maintained at about 10. Finally, the precipitated Fe_3O_4 magnetic particles were washed with distilled water until the pH value descended to 7.0, and were collected in vacuum drying chamber after being dried for 4 h at 60°C. The surface treatment was performed using an excess of oleic acid (added during 20 min) for an hour at 80°C. The black precipitate was then washed, dried and dispersed in cyclohexane to make dispersion with solid content 2.3%. The iron oxide prepared by this method was described by the following equations and was designated as o-Fe_3O_4.

$$Fe^{2+} + 2OH^- \longrightarrow Fe(OH)_2 \quad (1a)$$

$$3Fe(OH)_2 + {}^1\!/_2O_2 \longrightarrow Fe_3O_4 + 3\,H_2O \quad (1b)$$

2.2.2. *Preparation of Latex Particles by Inverse Mini-emulsion Polymerization*

All chemicals used in this study were divided into two parts including a dispersed phase and a continuous phase. The ingredients are shown in Table 1. In the preparation of the dispersed phase, the crosslinking agent EGDMA, the monomers, deionized water, and Tween 60 were mixed under continuous stirring. The total monomers concentration was 50%. The well-mixed dispersed phase was then introduced to the continuous phase solution, namely, Span 60/cyclohexane (CH) mixture, under stirring in an ice bath (0–5°C) for 20 min. After that, APS solution was introduced to the mixture solution slowly under stirring for an additional 30 min. The polymerization proceeded rapidly within several minutes. However, in order to ensure a maximum conversion of monomers, the reaction time was kept for roughly 30 min. The latex particles were precipitated using acetone and dried in a vacuum oven at 60°C until the sample weight remained constant. The same procedure was used in the case of the composite synthesis except that cyclohexane suspension of magnetite was used instead of cyclohexane in the continuous phase solution. The concentration of magnetite was the same for all synthesized composites. Pn and Mn are denoted to the naked polymer i.e., in absence of any magnetic particles and its corresponding magnetic composite, respectively.

2.2.3. *Characterization*

FTIR spectra of polymers were recorded in KBr pellets on Nicolet5700 FTIR THERMO. Powder X-ray diffraction (XRD, MAC, MXP21VAHF, Co–K) was used to investigate the crystal structure of the samples. For morphological characterization, scanning electron microscopy (SEM) Jeol JSM-5400 (JEOL, Tokyo, Japan) was used. The JEM-2000EX transmission election microscope (TEM) was used at an acceleration voltage of 200 kV. Thermograms of the polymeric nanogels and composites were recorded at a

Table 1. Synthesis recipes for the different polymer composites*

Sample code	*M1*	*M2*	*M3*	*M4*	*M5*	*EGDMA*	*Tween 60*	*APS*	*Span 60*	*H_2O:CH*
Am (moles)	1	3	1	1	—	24%	2%	10%	14%	1:3
SSASS (moles)	—	1	1	3	1					

*All ingredients were added based on the weight of monomer(s) which was constant through all the experimental work.

heating rate of 10°C/min up to 1000°C under N_2 conditions using a SDT Q600 (TA Co., USA) thermogravimetric analyzer.

The magnetic properties were studied with a vibrating sample magnetometer (9600 VSM, BDJ Electronics, Inc., Troy MI) at room temperature. Dynamic light scattering (DLS) measurements were performed in a laser scattering spectrometer (Submicron Particle Size Analyzer, Beckman Coulter-USA) equipped with a digital correlation (BI-10000 AT) at 20°C and the scattering angle for the DLS measurement was 11°. All the samples were prepared from aqueous suspension with a concentration of about 1 mg/ml and a diluent's viscosity of 0.01002poise. The mean particle size (nm) and the polydispersity index of the size distribution were obtained by the cumulated analysis.

3 Results and Discussion

3.1 Surface Treatment of Magnetite by Oleic Acid

In general, the role of surface treatment agents is to increase the hydrophobicity of iron oxide particles and to disperse these particles in the monomer droplets during the polymerization. Furthermore, the steric stabilization of these surface modifiers also provides entropic repulsion needed to overcome the short-range van der Waals attraction that otherwise results in irreversible particle aggregation. So, it is important to ensure that the modifiers are adsorbed on the surface of iron oxide particles (23). The adsorption of oleic acid onto Fe_3O_4 particles was confirmed by FTIR as shown later.

3.2 Synthesis of Polymers and Polymer Composites

The complexity of the particle nucleation mechanism and the difficulties in controlling the dispersion stability of inorganic particles in the continuous or disperse phase during emulsification and encapsulation polymerizations appear to be the major obstacles in preparing magnetic polymer microspheres with high encapsulation efficiency and high magnetic response. The characteristic features of the miniemulsion polymerization provide potential advantages for the polymer encapsulation of inorganic particles in the resulting latex particles (23).

Ammonium persulfate (APS) has anionic groups in the structure so it can decompose in the aqueous phase and form oligomeric radicals with a slightly dissolving monomer. The reaction rate increases with lowering pH and so the reaction is auto-accelerated during the polymerization. The polymerization initiated by hydroxyl radicals resulting from Equation 2 causes the formation of polymer particles with low surface charge, which decreases the electrostatic repulsive force between particles (9).

$$SO_4^{\cdot -} + H_2O \longrightarrow HO\cdot + SO_4^{2-} + H^+ \qquad (2)$$

In the presence of an additive, highly water-insoluble, low molecular weight compound so called hydrophobe (span 60 in this work), the molecular diffusion of the droplets is retarded, thus small droplets in mini-emulsions become stable. Surfactants also depress coalescence of droplets caused by mutual collisions (9, 24).

It was postulated for another system utilizing acrylic acid and sodium acrylate monomers and the inverse miniemulsion technique that the particle nucleation and growth loci were mainly in original droplets and only a small amount of particles was produced from homogeneous nucleation when NaOH was used as the costabilizer and the surfactant concentration was less than its CMC value. NaOH not only introduced the osmotic pressure but also increased the hydrophilicity of the monomer by ionization, which retarded the Ostwald ripening and increased the stabilization of the droplets (25).

SSASS received great attention in recent years due to its strongly ionizable sulfonate group. The synthesis of Am/SSASS via radical chain polymerization is a well-established procedure. SSASS dissociates completely in the overall pH range, and therefore, it might enhance the droplets' stabilization during the polymerization.

3.3 Acid-resistance of the Magnetic Composites

An acid-resistant experiment of magnetic composite particles was done by dispersing certain weight of magnetic nanogels in 5 mL of 1M HCl. Also, the same experiment was performed for Fe_3O_4 as the control one. After 5 h, magnetic composites were not dissolved. After separating magnetic nanogels by a magnet, the solution was colorless and transparent. It did not turn reddish when several droplets of KSCN solution were dropped in it. It meant that Fe_3O_4 may be tightly embedded in the highly crosslinked polymer networks and could not be eroded. In the control experiment, Fe_3O_4 was dissolved completely and the solution changed from yellow to red when the KSCN solution

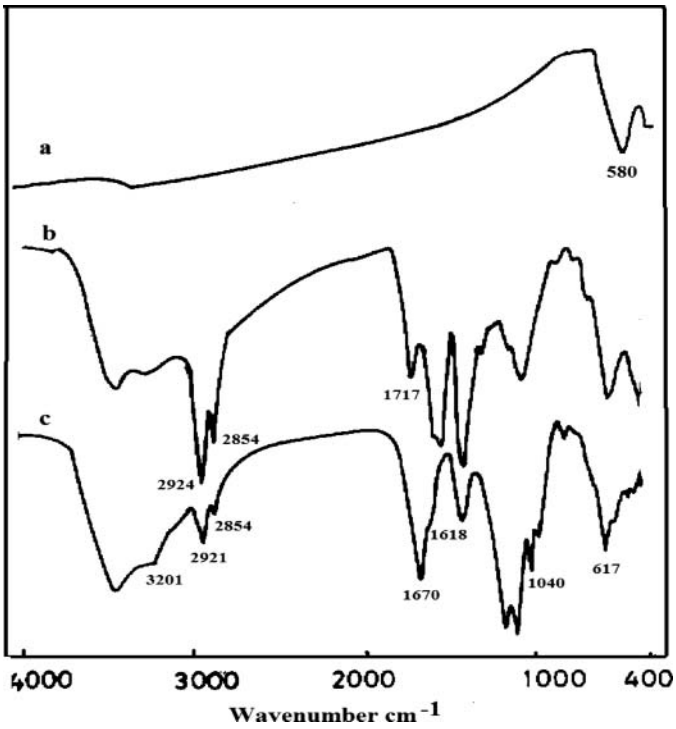

Fig. 1. Infrared spectra of (a) naked Fe_3O_4; (b) o-Fe_3O_4 and (c) the magnetic polymer composite M2.

was added. Therefore, to a great extent, the magnetic composites were acid-resistant.

3.4 Infrared Spectroscopy

To realize the binding mechanism, FTIR spectra of the naked Fe_3O_4; o-Fe_3O_4 and the magnetic polymer composite M2, were examined as shown in Figure 1(a-c), respectively. As a metallic oxide compound, naked iron oxide had rare absorbance bands in the spectrum and only the peak at 580 cm^{-1}, relates to Fe–O group, displayed. After the treatment with oleic acid, the o-Fe_3O_4 curve displayed new absorption peaks at 1717, 3238, 2854 and 2924 cm^{-1} corresponding to the C=O, –OH, C=C and $–CH_2–$groups in oleic acid, respectively. The absorption peak of Fe_3O_4 was clearly visible in the figure. This indicates a chemical adsorption of the oleic acid on the Fe_3O_4 surface.

With respect to the magnetic composite M2, the peaks at 1670 and 1618, 2921 and 3201 cm^{-1} may be correlated to the absorbance of the stretching vibration of the carbonyl group, the scissor vibration of $–NH_2$ of acrylamide, the aliphatic and aromatic hydrogens, respectively. The characteristic peak of SO group displayed at 1040 cm^{-1}. Also, the band corresponded to C=C of oleic acid at 2854 cm^{-1} was intact, this indicates that oleic acid did not participate in the polymerization process. However, when the size of Fe_3O_4 particles was reduced to the nano-scale dimensions as shown below by DLS, the surface bond force constant increased due to the effect of finite size of nanoparticles,

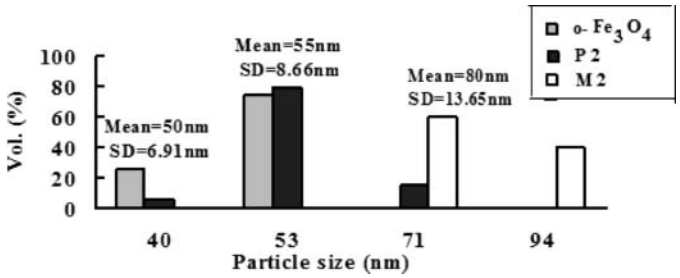

Fig. 2. Particle size distribution of o-Fe_3O_4; nacked polymer P2 and the polymer composite M2.

in which the breaking of large number of bonds for surface atoms resulted in the rearrangement of nonlocalized electrons on the particle surface (2). Therefore, the FTIR spectrum of iron oxide nanoparticles and nanogel magnetic particles would exhibit a blue shift and the characteristic absorption bands of Fe–O bond were shifted to a higher wavenumber of about 617 cm^{-1}. In conclusion, iron oxide was successfully encapsulated in the synthesized copolymer.

3.5 Polydispersity and Mean Particle Size

Figure 2 shows the particle size distribution of the o-Fe_3O_4, the naked polymer P2 corresponding to M2 and the polymer composite M2, respectively. The mean particle size was 50, 55 and 80 nm, for o-Fe_3O_4, P2 and M2, respectively. The percentage ratios of the standard deviation "SD" to the mean size of the particle distribution were 13.8, 15.7 and 17%, respectively, considering finite error in the statistical distribution of the particle sizes. The polydispersity for them exceeded 0.5, indicating non-uniform particles size which may be attributed to the coagulation of the particles due to the static electron interaction and the small-size effect (24).

Besides, the dissociation of APS, based on Equation 2, enhanced the ionic strength in the aqueous system, and suppressed the electrical double layer around the particles. Thus, magnetic particles would coalesce with each other owing to the gradual hydrolysis of persulfate ion radical. The high concentration of APS was responsible for the large composite particles (9). Nevertheless, to reduce coagulation phenomenon is an issue that needs to be studied further for obtaining mono-disperse nanometeric-size particles.

3.6 X-ray

Figure 3 (a and b) shows the XRD patterns for the o-Fe_3O_4 and the polymer composite M2, respectively. Six characteristic peaks for Fe_3O_4 marked by "m" were observed for both samples. These peaks were consistent with the database in JCPDS file (PDF No.65-3107) and revealed that the resultant particles were pure magnetite. It is also explained that both the surface treatment process and the encapsulation

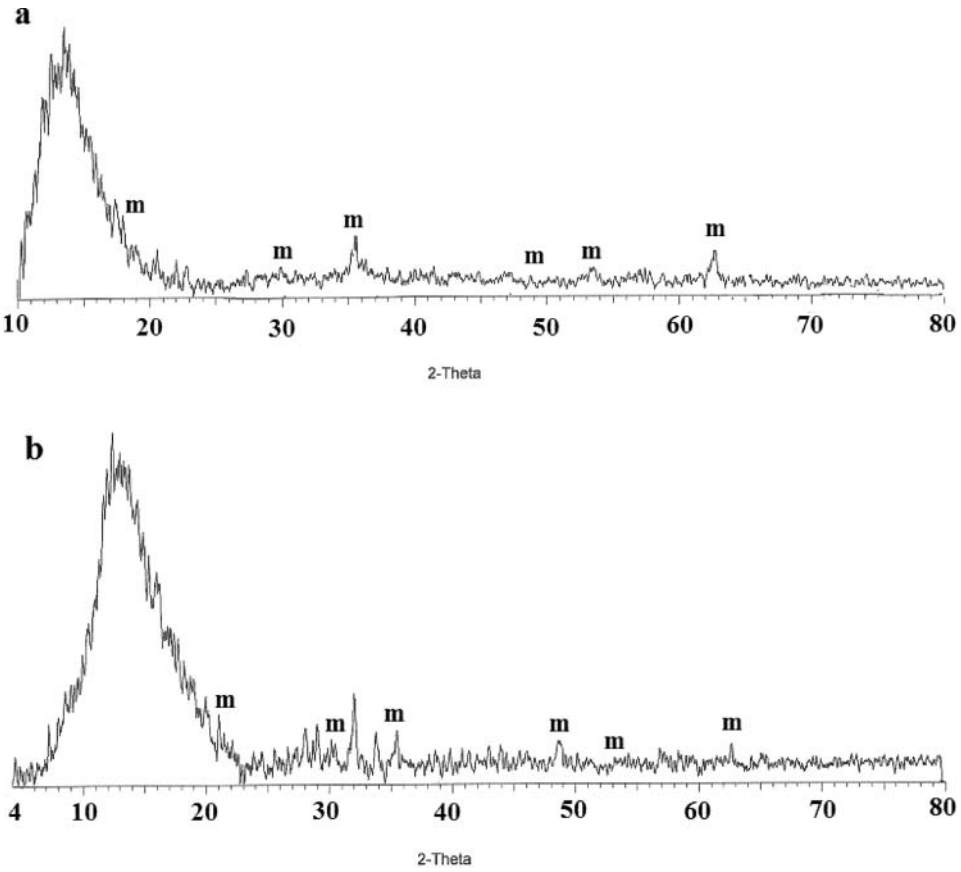

Fig. 3. X-ray diffraction for a) o-Fe_3O_4 and, b) polymer composite M2.

processes did not result in any phase change or oxidation of Fe_3O_4 during these interactions. The broad nature of the diffraction bands in the X-ray pattern was an indication of the small particle size.

3.7 Thermal Analysis

The formation of nanocomposites is usually related to the change in thermal properties of the polymer (26). The thermal stability is the ability of a material to maintain its physical properties when exposed to high temperatures and is generally estimated from the weight loss upon heating which results in the formation of volatile products (27).

Figure 4 (a and b) shows the TGA curves for the naked copolymer P2 corresponding to M2 and the polymer composite M2, respectively. The thermal degradation curve of P2 showed three weight loss stages. Desorption of the physically adsorbed water occurred at 100°C, while that absorbed by the polymer by different binding modes might evaporate at higher temperatures during the first stage. Generally, the thermal degradation of polymers includes three steps. In the first step, the polymer thermal degradation was initiated by scissions of head-to-head linkages (H–H) at 140–160°C, depending on the heating rate. The second step (200–300°C) was initiated by scission at the vinylidene chain-end units and the third step (above 300°C) by random scission within the polymer chain (26), accordingly, the onset of the polymer backbone cleavage or so-called carbonation was probably in the second stage. The last step can be attributed to the further degradation of polymer residues to yield carbon and hydrocarbons. The thermograms of the ferrogels also showed three main weight loss stages, neglecting the one corresponding to the physically adsorbed water. It is worth mentioning that the onset of oleic acid degradation may be in the second stage. The main observations that can be made are the following:

(i) The weight loss in the second stage at 600°C, which is concerned with the polymer degradation, for P2 was higher than that for M2 by about 15%. Thus, the nanoparticles might act as a heating barrier and might induce the polymer-filler interactions, which could reduce the diffusion of the decomposition products and could restrict the polymer chain mobility. In the present case, the polymer nanoparticles interaction could be a type of adhesive forces, this kind of interaction has been accepted by several authors to exist between magnetite particles and a polymer in a nanocomposite (28).
(ii) The residual weight at 1000°C for M2 and P2 were 26.25 and 12.96%, which corresponded to the magnetite

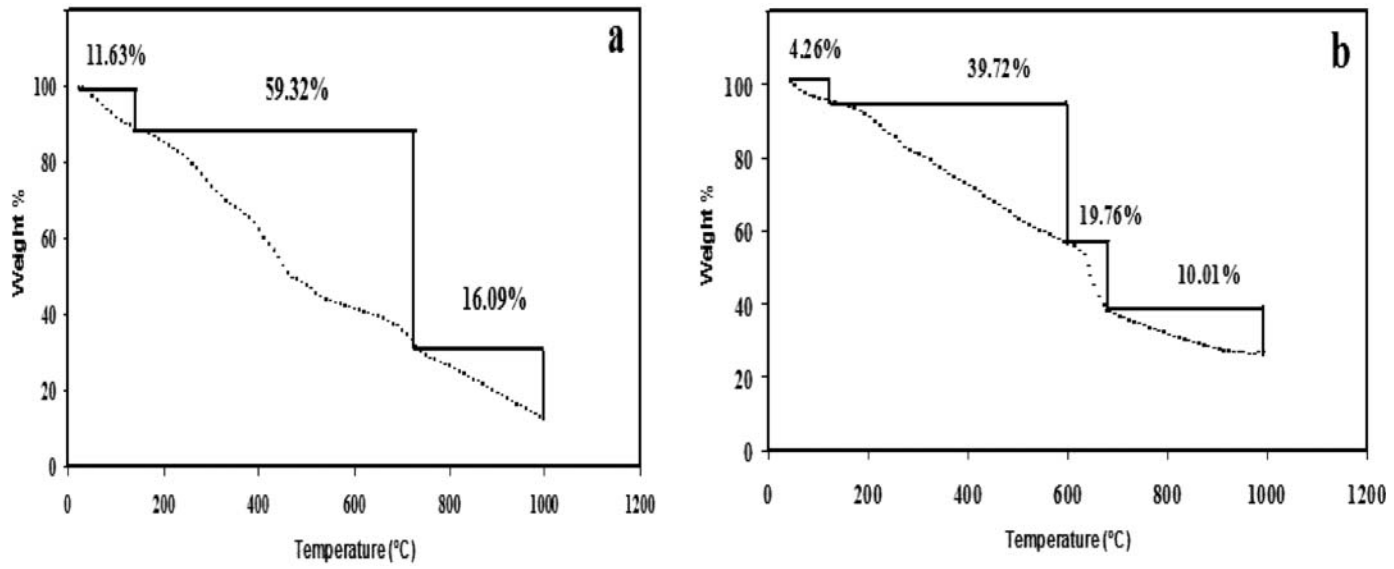

Fig. 4. TGA of a) the naked polymer P2 and b) the polymer composite M2.

nanoparticles and the char yielded by the copolymer, respectively. This may be further clear proof on the enhancement of the thermal stability of the prepared composite.

3.8 Surface Morphology

The spherical morphology of nanocomposite particles was determined by SEM as shown in Figure 5(a) while Figure 5(b) shows the TEM of the polymer composite particles M2; as observed, these particles were definitely spherical but rather polydisperse. The nano-sized magnetite particles were visible as dark spots inside the spherical polymer nanospheres. Also, the magnetite particles were covered by the polymeric shell. However, the ease of aggregation of the magnetite particles appeared to make the formation of individual polymer covered magnetite units difficult, and it seems more likely that a single polymer shell enclosed more than one magnetite particle.

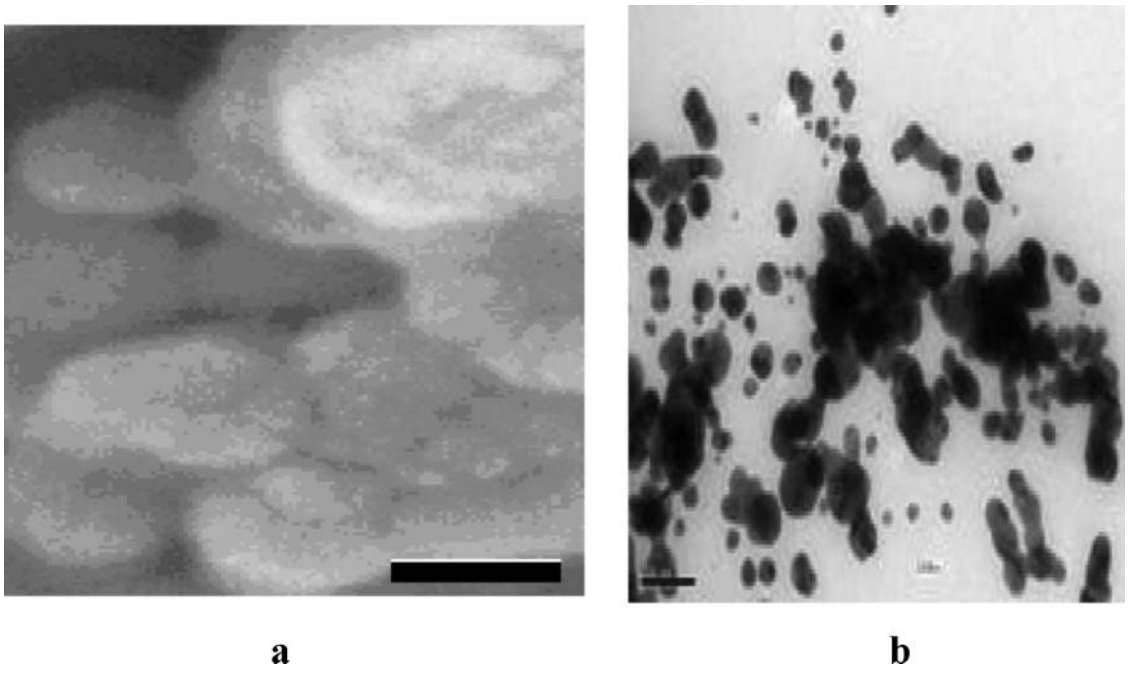

Fig. 5. SEM (a) and TEM (b) of polymer composite M2, the scale bar was 100 nm.

Table 2. The magnetic properties of the synthesized iron oxide and composites

Sample code	H_c *(Oe)*	M_r *(emu/g)*	M_s *(emu/g)*
o-Fe_3O_4	87.37	1.375	7.908
M1	50.33	0.333	2.937
M2	55.66	0.529	3.557
M3	58.36	0.235	1.508
M4	51.04	0.152	1.260
M5	52.46	0.152	1.317

3.9 Magnetic Properties

The characters of polymer chains, functional groups and the morphology of the composite have effects on magnetic properties of composite particles (9).

Magnetic hysteresis loops are commonly employed to describe the properties of magnetic materials. In magnetometry, the magnetization of the material, M, is measured relative to the applied field, H. When a sufficiently large field is applied, the majority of spins within the material align with the field. The magnetization in these cases is described as the saturation magnetization, M_s. As the field is reduced, the spins in the material no longer align perfectly with the field, and some spins remain aligned at zero field. The magnetization at that point is described as the remanent magnetization; M_r. The field is further decreased until the magnetization becomes zero. This point is the coercive field, H_c. This is the magnitude of field that must be applied to bring the net moment of the sample to zero.

Figure 6(a-b) illustrates typical hysteresis loops for o-Fe_3O_4 and the polymer composite M2, respectively. The magnetic properties of the synthesized iron oxides and the composites are represented in Table 2.

Many remarks can be observed as follows. (i) the ionic monomer content also influenced the magnetic behavior of the prepared composites, (ii) the prepared composites possessed a certain level of magnetic response, (iii) the large coercivity of iron oxide resulted in a much large hysteresis loss and (iv) although, the prepared magnetite and the magnetic composites did not follow the scenario of superparamagnetic materials in which M_r and H_c equal to zero, the magnetic composites may be potentially applicable in many fields other than medical ones such as printing inks, magnetic recording material and catalysts. For example, for optimum performance in magnetic recording material, the particles should exhibit both high coercivity and high remanence, and they should be uniformly small, and resistant to corrosion, friction, and temperature changes (29). The decrease of the saturation magnetization is most likely attributed to the existence of span-60 on the surface of Fe_3O_4 nanoparticles which might create a magnetically dead layer. With a significant fraction of surface atoms, any crystalline disorder within the surface layer might also lead to a significant decrease in the saturation magnetization of nanoparticles (30). The obtained results are comparable with those

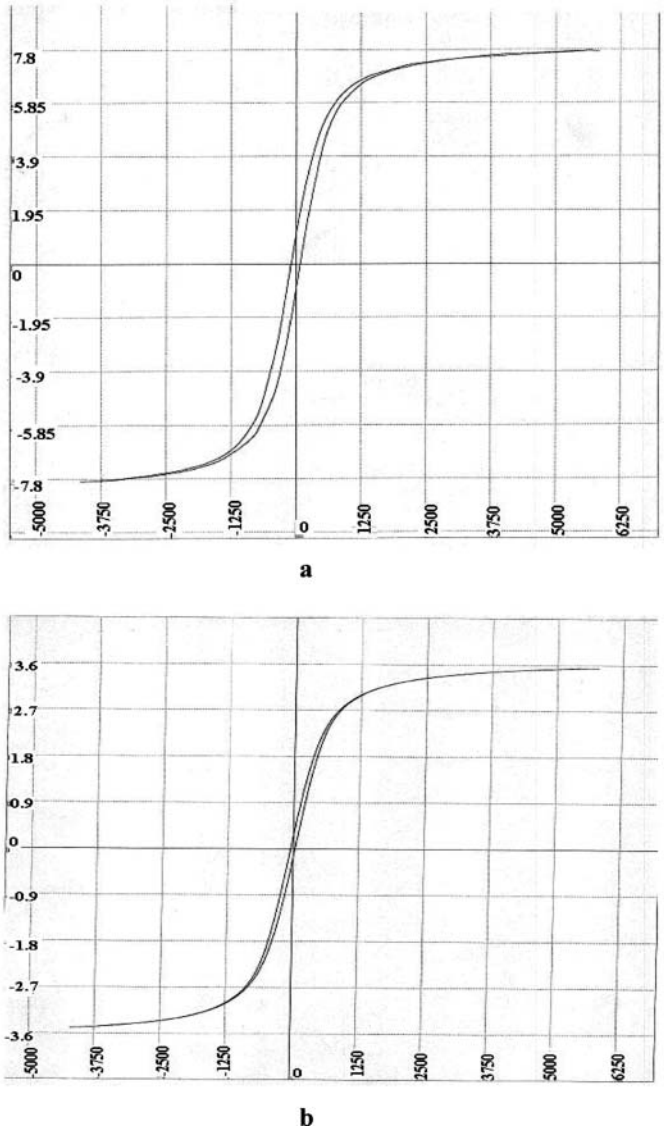

Fig. 6. Magnetization (emu/g) vs. applied magnetic field (kOe) for a) o-Fe3O4 and, b) the polymer composite M2.

obtained for Fe_3O_4/SiO_2/PMAA tri-layer microspheres (31) and for magnetic styrene composite nanoparticles prepared by seeded emulsion polymerization (7).

It is worthy to mention that particles which can freely rotate during magnetometry experiments will appear as though they have superparamagnetic behavior, due to randomization caused by particle rotations. However, if the particles are held rigidly in place, some coercivity may be observed (29).

The increase of H_c may be due to the higher anisotropy expected in iron oxide nanoparticles. A strong magnetic interaction between the particles may result in ordering of the magnetic moments of the particles, which would be super-paramagnetic if they were non-interacting. This is a so-called super-ferromagnetic state. It is valuable to mention that transformation to super-paramagnetism may

be attained by reducing the magnetic interaction between the particles via coating the nanoparticles with a polymer layer whose steric repulsion is greater than or equal to the magnetic interaction between the particles, which increases the repulsion between two magnetic nanoparticles. The limitation associated with this method is that there are very few biopolymers that are hydrophilic, surfactant- like and have a single reactive end-group for attaching to the Fe surface (32).

4 Conclusions

Encapsulation or dispersion of magnetic nanoparticles into organic polymers to form magnetic composite particles endows particles with some important properties that bare uncoated particles lack. Polymer coatings can enhance compatibility with organic ingredients, reduce susceptibility to leaching, and protect particle surfaces from oxidation. In this manuscript, inverse miniemulsion polymerization of acrylamide and styrene sulfonic acid sodium salt was a successful technique to encapsulate, *in situ*, magnetite nanoparticles. Many remarks can be highlighted as follows:

1. The magnetic composites were acid-resistant.
2. Infrared spectroscopy confirmed that iron oxide was successfully encapsulated in the synthesized copolymer.
3. XRD proved that the prepared iron oxide was magnetite and both the coating process and the encapsulation processes did not result in any phase change or oxidation of magnetiteduring the surface treatment or the polymerization reaction.
4. The encapsulated magnetite enhanced the thermal stability of the polymer composites.
5. Magnetic composites were proven to be superferromagnetic.
6. The production of large quantities of magnetic nanoparticles with narrow size distribution remains a significant challenge.

References

1. Ménager, C., Sandre, O., Mangili, J. and Cabuil, V. (2004) *Polymer*, 45, 2475–2481.
2. Khan, A. (2008) *Mater. Lett*., 62, 898–902.
3. Li, G., Jiang, Y., Huang, K., Ding, P. and Chen, J. (2008) *J. Alloy Compd*., 466, 451–456.
4. Paneva, D., Stoilova, O., Manolova, N. and Rashkov, I. (2004) *e-Polymers*, 60, 1–11.
5. Deng, Y., Wang, L., Yang, W., Fu, S. and Elaïssari, A. (2003)) *J. Magn. Magn. Mater.*, 257, 69–78.
6. Liu, G., Wang, H. and Yang, X. (2009) *Polymer*, 50, 2578–2586.
7. Lu, S., Qu, R. and Forcada, J. (2009) *Mater. Lett*., 63, 770–772.
8. Kondo, A., Kamura, H. and Higashitahi, K. (1994) *Appl. Microbiol. Biotechnol*., 41, 99–105.
9. Mori, Y. and Kawaguchi, H. (2007) *Colloid Surface B*, 56, 246–254.
10. Lu, S., Ramos, J. and Forcada, J. (2007) *Langmuir*, 23, 12893–12900.
11. Faridi-Majidi, R., Sharifi-Sanjani, N. and Agend, F. (2006) *Thin Solid Films*, 515, 368–374.
12. Cocker, T., Fee, C. and Evans, R. (1997) *Biotechnol. Bioeng.,* 53, 79–87.
13. Sun, H., Yu, J., Gong, P., Xu, D., Zhang, C. and Yao, S. (2005) *J. Magn. Magn. Mater*., 294, 273–280.
14. Mefford, O., Carroll, M., Vadala, M., Goff, J., Mejia-Ariza, R., Saunders, M., Woodward, R., Pierre, T., Davis, R. and Riffle, J. (2008) *Chem. Mater.,* 20, 2184–2191.
15. Chatterjee, J., Haik, Y. and Chen, C. (2004) *Bio. Magn. Res. Technol.,* 2, 1–3.
16. Liu, X., Liu, H., Xing, J., Guan, Y., Ma, Z., Shan, G. and Yang, C. (2003) *China Particuol*, 1, 76–79.
17. Bayramoğlu, G., Yılmaz, M., şenel, A. and Arıca, M. (2008) *Biochem. Eng. J.,* 40, 262–274.
18. Ang, B. and Iskandar, I. (2007) *J. Mater. Process Technol.*, 191, 235–237.
19. Bee, A., Massart, R. and Neveu, S. (1995) *J. Magn. Magn. Mater.,* 149, 6–9.
20. Cai, W. and Wana, J. (2007) *J. Colloid Interf. Sci.*, 305, 366–370.
21. An, L., Li, Z., Li, W., Nie, Y., Chen, Z., Wang, Y. and Yang, B. (2006) *J. Magn. Magn. Mater.*, 303, 127–130.
22. Yuanbi, Z., Zumin, Q. and Jiaying, H. (2008) *Chinese J. Chem. Eng.,* 16, 451–455.
23. Zhang, Q., Zhang, H., Xie, G. and Zhang, J. (2007) *J. Magn. Magn. Mater.,* 311, 140–144.
24. Ma, P., Xiao, C., Li, L., Shi, H. and Zhu, M. (2008) *Eur. Polym. J.,* 44, 3886–3889.
25. Luo, Y., Dai, C. and Chiu, W. (2009) *J. Colloid Interf. Sci*., 330, 170–174.
26. Huskic, M. and Žigon, M. (2007) *Eur. Polym. J.,* 43, 4891–4897.
27. Zeng, Q., Yu, A., Lu, G. and Paul, D. (2005) *J. Nanosci. Nanotechnol.,* 5, 1574–1592.
28. Goiti, E., Salinas, M., Arias, G., Puglia, D., Kenny, J. and Mijangos, C. (2007) *Polym Degrad. Stabil*., 92, 2198–2205.
29. Teja, A. and Koh, P. (2009) *Prog. Crys Growth Ch. Mater.,* 55, 22–45.
30. Ang, K., Venkatraman, S. and Ramanujan, R. (2007) *Mater. Sci. Eng. C*, 27, 347–351.
31. Liu, G., Wang, H. and Yang, X. (2009) *Polymer*, 50, 2578–2586.
32. Balakrishnan, S., Bonder, M. and Hadjipanayis, G. (2009) *J. Magn. Magn. Mater.*, 321, 117–122.